



Observation of surface displacements from GPS analyses before and after the Jiashian earthquake ($M = 6.4$) in Taiwan

Chieh-Hung Chen^{a,b,*}, Strong Wen^c, Ta-Kang Yeh^d, Chung-Ho Wang^a,
Horng-Yuan Yen^e, Jann-Yenq Liu^{f,g}, Yasuhide Hobara^{b,h}, Peng Hanⁱ

^a Institute of Earth Sciences, Academia Sinica, Taipei 115, Taiwan, ROC

^b Research Station on Seismo-Electromagnetics, UEC, Chofu, Tokyo, Japan

^c National Center for Research on Earthquake Engineering, Taipei 106, Taiwan, ROC

^d Department of Real Estate and Built Environment, National Taipei University, New Taipei City 237, Taiwan, ROC

^e Institute of Geophysics, National Central University, Jhongli 320, Taiwan, ROC

^f Institute of Space Science, National Central University, Jhongli 320, Taiwan, ROC

^g Center for Space and Remote Sensing Research, National Central University, Jhongli 320, Taiwan, ROC

^h Department of Communication Engineering and Informatics, Graduate School of Informatics and Eng., UEC, Chofu, Tokyo, Japan

ⁱ Graduate School of Science, Chiba University, Inage, Chiba 263-8522, Japan

ARTICLE INFO

Article history:

Received 12 June 2012

Received in revised form 24 October 2012

Accepted 4 November 2012

Available online 29 November 2012

Keywords:

Global positioning system

Hilbert–Huang transform

Jiashian earthquake

ABSTRACT

A blind thrust fault with a unique strike, which is orthogonal to the strike of most tectonic structures in Taiwan, triggered the Jiashian earthquake on March 4, 2010 ($M = 6.4$; 22.96°N , 120.70°E). This study utilizes 100 global positioning system stations to examine changes of surface displacements during the Jiashian earthquake. We mitigate effects of short-term noise and long-term plate movements from surface displacement data using a frequency dependent filter via the Hilbert–Huang transform and compute the horizontal azimuth (i.e. GPS-azimuth) using residual data at the NS component relative to residual data at the EW component. Analytical results show that orientations of horizontal azimuths were aligned and orthogonal to the strike of the blind thrust fault. Meanwhile, inverse orientations are observed before and after the earthquake that agrees well with the seismic rebound theory. As stress disturbed on strata a few days before the earthquake, an impeded region can be clearly identified by disordered orientations of horizontal azimuths for anticipating the mainshock. These results provide an additional view to explore stress disturbance associated with earthquakes and offer more information to examine diverse models of tectonic evolution in this region.

© 2012 Elsevier Ltd. All rights reserved.

1. Introduction

Taiwan is located in the western margin of the circum-Pacific seismic belt. The Philippine Sea plate with an average rate of about 8 cm/yr (Yu et al., 1997) moves toward a NW direction and intensely interacts with the Eurasia plate that results in the creation of most tectonic structures with a particular strike of a NNE–SSW trend (Ho, 1988) as well as numerous earthquakes. On March 4, 2010, the Jiashian earthquake ($M = 6.4$; 22.96°N , 120.70°E) occurred about 17 km southeast away from the Jiashian township (23.08°N , 120.59°E) of Taiwan (Fig. 1). Magnitude of this earthquake is not rare in high seismicity Taiwan but the strike of fault judged from the aftershock distribution is orthogonal to the NNE–SSW strike of most tectonic structures that has attracted

* Corresponding author at: Institute of Earth Sciences, Academia Sinica, Taipei 115, Taiwan, ROC. Tel.: +886 2 2783 9910x523; fax: +886 2 2783 9871.

E-mail address: nononochchen@gmail.com (C.-H. Chen).

considerable attention by many scientists (Ching et al., 2011; Wen et al., 2012; Chan and Wu, 2012; Lee et al., in press). The Jiashian earthquake located near the southwestern fold-and-thrust belt and occurred at a focal depth of about 22 km beneath the southern Central Range of Taiwan (Fig. 1). The focal mechanism of the Jiashian earthquake retrieved from BATS (Broadband Array in Taiwan for Seismology at <http://bats.earth.sinica.edu.tw/>) indicates a sinistral thrust mechanism (the P -axis trending NNE–SSW). The strike and the dip of the fault plane are 318° and 41° to the NE, respectively (Fig. 1). It is well known that surface displacements using global positioning system (GPS) data are often employed as a boundary condition in studying fault rupture processes (Peltzer et al., 1998; Barbot et al., 2008; Barbot and Fialko, 2010). Since surface displacements during earthquakes are highly associated with faults, temporal variation of surface displacement provides an excellent opportunity to expose seismogenic processes of this unique event (i.e. the Jiashian earthquake) in this study.

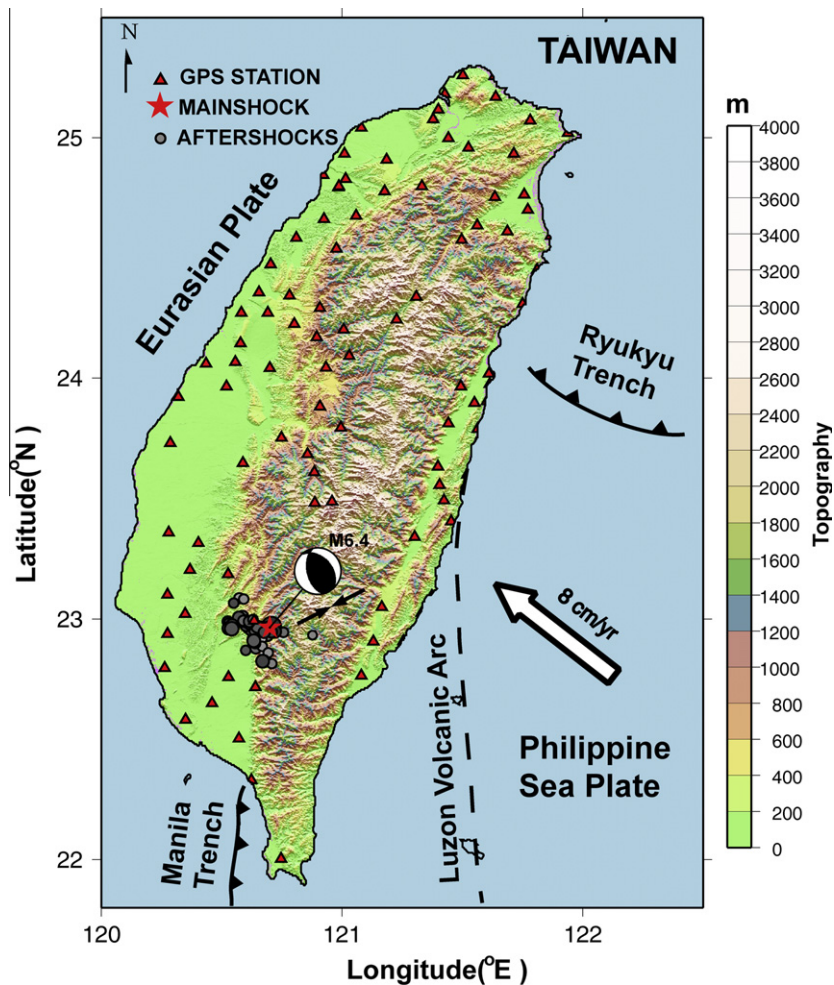


Fig. 1. The topography and tectonic structure in the Taiwan region and location of the Jiashian earthquake. The red star and grey circles denote the mainshock and aftershocks of the Jiashian earthquake, respectively. The red triangles show the location of GPS stations used in this study. (For interpretation of the references to color in this figure legend, the reader is referred to the web version of this article.)

Continuous GPS data have been considered to be integrated by numerous signals. The trend of long-term GPS data generally stands for large-scale plate movements (Reilinger et al., 1997; McClusky et al., 2003; Prawirodirdjo and Bock, 2004; Wernicke et al., 2004; Geirsson et al., 2006). Instantaneous dislocation and/or step changes lie on long-term variations that are generally related to co-seismic displacements of earthquakes (Yu et al., 2001; Gahalaut et al., 2006). Changes of the long-term trend after earthquakes are often considered to be post-seismic deformation due to the elastic and/or viscoelastic rebound (Wang, 2007). Furthermore, influences from the ionosphere and atmosphere on GPS data would yield obvious semi-annual and annual cycles (Van Dam et al., 2001; Blewitt and Lavallee, 2002; Ray et al., 2008; Yeh et al., 2008). It is difficult to retrieve more valuable signals from GPS data without removal of these aforementioned disturbances. To understand accumulation and release of stress during earthquakes, Chen et al. (2011) mitigated these aforementioned well-known effects by using a band pass filter via the Hilbert–Huang transform (Huang et al., 1998) to adapt a non-linear and non-stationary nature. Chen et al. (2011) found that orientations of horizontal displacements deduced from residual GPS data are aligned toward a similar direction just a few days before and after earthquakes. Aligned orientations are orthogonal to strikes of reverse faults and yield inverse rotation before and after thrust earthquakes that are consistent with the seismic

rebound theory (Reid, 1910). Although co-seismic (step) changes would slightly disturb analytical results, orientations of horizontal displacements computed from filtered data are consistent with parameters of seismic fault and/or focal mechanisms. Evolution of the orientations has been repeatedly observed in many thrust earthquakes in Taiwan and Japan, and can provide valuable information in understanding earthquake-related stress disturbance.

This study employs the method in Chen et al. (2011) to filter long-term plate movements, short-term noise and frequency dependent (i.e. semi-annual and annual) variations from the 100 GPS stations (retrieved from Central Weather Bureau; <http://www.cwb.gov.tw>) in Taiwan. The residual GPS data in the horizontal components are utilized to compute orientations of horizontal displacements. An inverse value of an average, which is computed from difference of the orientations between every two stations within a spatially moving window, is determined to be the GPS index. Time-shifting maps constructed by the spatial-shifting GPS index on 20 days before and 29 days after the Jiashian earthquake are used to understand varied situation of stress disturbance and compared with parameters of the focal mechanism (retrieved from BATS) and distribution of aftershocks (retrieved from the Central Weather Bureau (CWB), Taiwan at <http://www.cwb.gov.tw>; also see Table 1), as well as those of previous studies for investigating valuable physical phenomena if any.

2. GPS data

Coordinates of daily solutions at 100 GPS stations (retrieved from CWB) are calculated with respect to the Kinmen (KMMN) site (located at 24.46°N, 118.39°E; <http://www.gps.moi.gov.tw/SSCenter/Introduce/InfoPage.aspx>) by assuming a static relative distance via Bernese 5.0 software (Dach et al., 2007) to process the double-differenced GPS phase observations. Note that we determined the precise coordinates of the KMMN station by using the International Terrestrial Reference Frame 2005 (ITRF2005) for geocentric coordinates. The tropospheric delay is corrected by using the Saastamoinen model (Saastamoinen, 1973) with an elevation-dependent

weighting of $\cos^2(z)$, where z is the zenith distance. Meanwhile, to estimate the wet delay of GPS signals in the zenith direction, an hourly wet tropospheric parameter is applied (Wang et al., 2008). We remove the ionospheric delay using a combination of GPS data at L1 and L2 frequencies, and satellite clock errors are removed using the International GNSS Service (IGS) precise ephemerides (Yeh et al., 2009).

3. Hilbert–Huang transform

The Fourier transform (Bracewell, 2000) and the wavelet transform (Daubechies, 1990) have been widely adapted for transferring

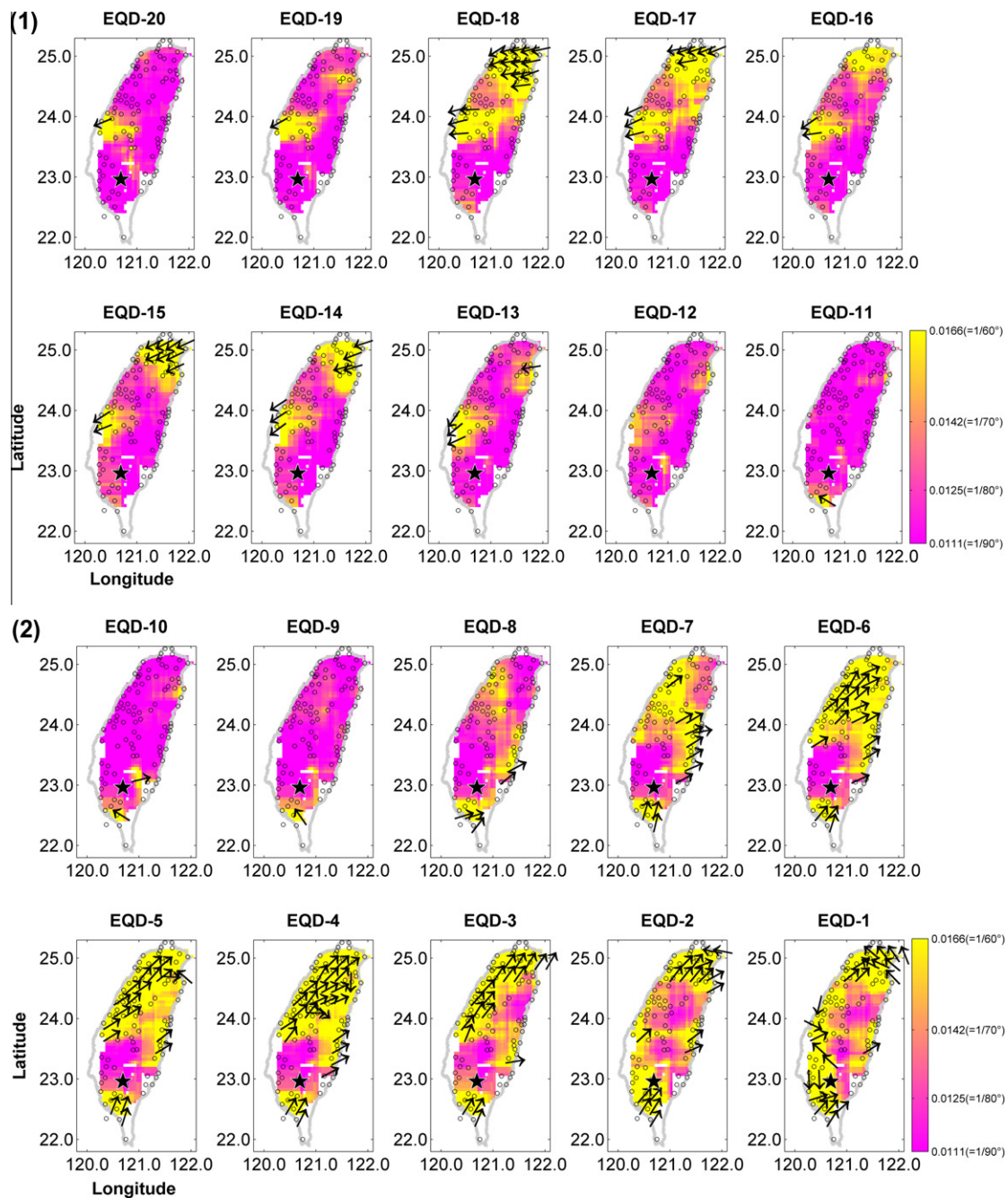


Fig. 2. Maps of the GPS index from 20 days before and 29 days after the Jiashian earthquake. The pink and yellow colors denote areas of small (~ 0.011) and large GPS indexes (~ 0.02), respectively. Black arrows show the direction of surface displacements. GPS stations used in this study are shown by open circles. The black star and blue crosses denote the mainshock and aftershocks of the Jiashian earthquake, respectively. (For interpretation of the references to color in this figure legend, the reader is referred to the web version of this article.)

time-series data into the frequency domain. Linear signals are a basic assumption of either the Fourier transform or the wavelet transform, but they are against a non-linear and non-stationary nature. This study uses the Hilbert–Huang transform (HHT) (Huang et al., 1998, 2003; Huang and Wu, 2008) to extract earthquake-related surface displacement signals for catching the non-linear and non-stationary nature. HHT is integrated by the Empirical Mode Decomposition (EMD) and the Hilbert transform. Time-series data can be decomposed into a series of intrinsic mode functions (IMFs) by using Sifting during the EMD process based on energy characteristics (details can be found in Huang et al., 1998). Regarding the Sifting processes, local maxima and minima of the analyzed data are found first and then connected as the upper and lower envelopes by using the cubic spline method, respectively. The difference

derived from the analyzed data and the average of the upper and lower envelopes is computed and then repeatedly removed from the analyzed data accordingly. The Sifting process would be temporally stopped once an average of the difference is less than 10^{-6} m. In this case, the difference is determined as IMF_1 and sequentially subtracted from the analyzed data accordingly. The subtracted data replace the analyzed data to obtain following IMF by using Sifting again. The Sifting process would be consequently stopped, while the upper and lower envelopes cannot be constructed by enough quantities of the local maxima and minima. Each of the derived IMFs is transferred into the frequency domain using the Hilbert transform. Thus, IMFs can be obtained from decomposed time-series data on surface displacement at each GPS station. Meanwhile, the instantaneous frequency and instantaneous amplitude in the

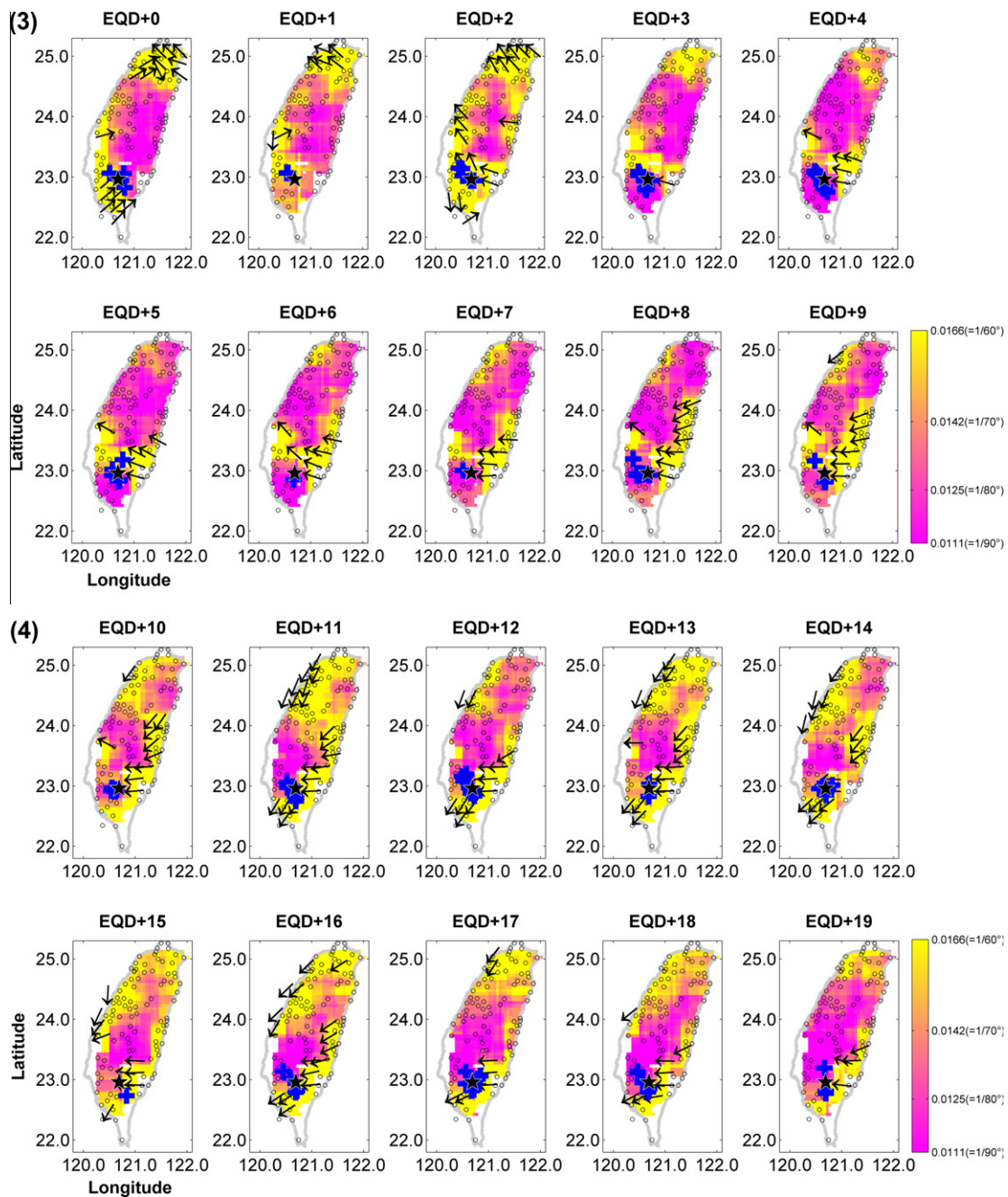


Fig. 2. (continued)

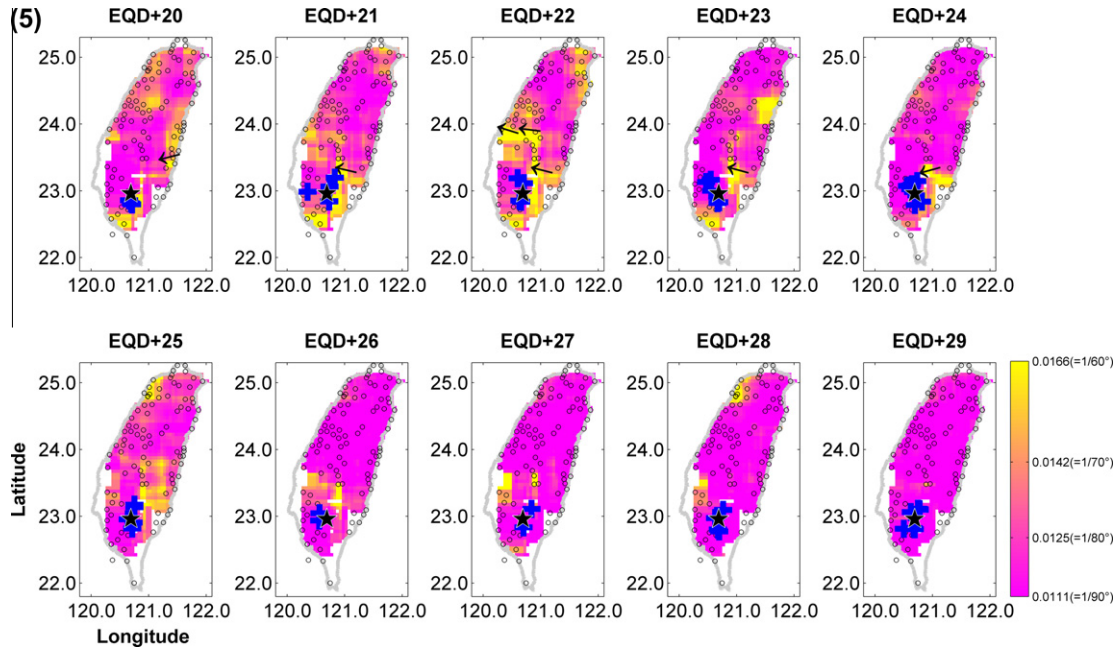


Fig. 2. (continued)

Table 1
The earthquake catalog regarding the mainshock and aftershocks ($M > 3$) of the Jiashian earthquake.

Year	Month	Day	Hour	Min.	Sec.	Long.	Lat.	Depth	Mag.
2010	3	4	0	18	52.1	120.707	22.969	23	6.4
2010	3	4	0	26	10.2	120.551	22.976	20	3.5
2010	3	4	0	24	47.3	120.622	22.984	20	4.7
2010	3	4	0	32	39.3	120.656	22.955	16	3.5
2010	3	4	0	43	26	120.636	22.96	17	3.7
2010	3	4	0	47	53.5	120.664	22.941	20	3.2
2010	3	4	0	54	52.1	120.628	22.962	17	3.7
2010	3	4	0	54	4.7	120.658	22.958	18	3.4
2010	3	4	0	58	22	120.66	22.951	19	3.5
2010	3	4	1	3	29.8	120.608	22.963	16	3.2
2010	3	4	1	3	7.1	120.595	22.995	17	3.3
2010	3	4	1	18	27	120.619	22.959	18	3.2
2010	3	4	1	23	22.8	120.653	22.957	17	3.1
2010	3	4	1	31	28.6	120.622	22.955	17	3.2
2010	3	4	1	57	55.6	120.641	22.962	17	3.6
2010	3	4	2	1	40.5	120.632	22.975	18	3.8
2010	3	4	2	18	54.6	120.525	22.99	21	3.5
2010	3	4	2	30	42.8	120.61	22.973	16	3.8
2010	3	4	2	32	36.6	120.667	22.964	20	3.9
2010	3	4	2	34	20	120.645	22.965	17	3.7
2010	3	4	2	43	36.1	120.603	22.972	16	3.7
2010	3	4	2	48	34.8	120.602	22.981	17	3.9
2010	3	4	3	47	33.6	120.616	22.959	17	3.4
2010	3	4	3	55	37.6	120.621	22.973	16	3
2010	3	4	3	58	26.3	120.646	22.96	17	3.3
2010	3	4	4	1	59.2	120.643	22.96	17	3.8
2010	3	4	4	29	6.7	120.612	22.966	16	3.2
2010	3	4	4	43	12.2	120.607	22.98	18	3.2
2010	3	4	5	24	9.8	120.586	23.012	16	3.8
2010	3	4	6	20	39.1	120.624	22.977	18	3
2010	3	4	6	30	31.1	120.654	22.958	18	3.7
2010	3	4	7	23	21	120.601	22.985	16	3.2
2010	3	4	8	7	59.7	120.618	22.973	17	4.4
2010	3	4	8	17	58	120.639	22.944	18	3.3
2010	3	4	8	18	52.2	120.637	22.949	18	3.4
2010	3	4	8	16	16.3	120.635	22.958	19	5.7
2010	3	4	8	27	18.1	120.658	22.96	18	4.3
2010	3	4	8	57	57.4	120.624	22.975	17	3.1
2010	3	4	9	24	1.4	120.693	22.969	21	3.4
2010	3	4	9	29	49.1	120.528	22.986	19	3
2010	3	4	9	38	31.3	120.629	22.956	17	3.3
2010	3	4	9	47	3.5	120.626	22.957	19	4.3

Table 1 (continued)

Year	Month	Day	Hour	Min.	Sec.	Long.	Lat.	Depth	Mag.
2010	3	4	9	51	24.5	120.636	22.952	18	3.2
2010	3	4	10	31	26.6	120.656	22.965	17	3.7
2010	3	4	11	12	25.6	120.601	22.974	18	3.7
2010	3	4	12	9	14.8	120.699	22.948	20	3.7
2010	3	4	16	5	58.3	120.571	23.006	18	4
2010	3	5	15	10	42.7	120.691	22.93	16	3.4
2010	3	5	16	5	32.6	120.691	22.949	20	3.4
2010	3	6	21	23	59.4	120.709	22.816	13	3.2
2010	3	7	9	0	32.9	120.574	23.087	10	3.5
2010	3	8	17	54	30.3	120.53	22.961	20	4.2
2010	3	9	5	31	47.3	120.648	22.968	17	4.1
2010	3	9	6	26	49.5	120.693	22.953	11	3.1
2010	3	9	11	27	44	120.665	22.918	8	3.4
2010	3	9	20	14	7	120.596	22.993	16	4.1
2010	3	9	20	17	27.3	120.59	22.993	15	3.5
2010	3	9	20	51	4.2	120.613	22.977	13	3
2010	3	13	9	15	33.6	120.616	22.99	18	3.7
2010	3	15	22	8	30.3	120.757	22.944	15	3.2
2010	3	22	22	26	55.3	120.722	22.949	23	4
2010	3	22	23	1	51.7	120.631	22.892	14	3.2
2010	3	24	8	33	28.8	120.642	22.878	15	3.6
2010	3	26	20	5	37.3	120.632	22.908	16	3
2010	3	27	5	8	18.5	120.669	22.886	11	3.3
2010	3	27	12	16	4.5	120.543	22.975	20	4
2010	4	2	20	44	45.5	120.693	22.861	11	3.2
2010	4	6	1	38	13	120.707	22.947	21	3.6
2010	4	14	21	37	6.4	120.627	22.914	17	3.1
2010	4	15	11	15	52.7	120.629	22.998	15	3.3
2010	4	23	17	3	23.2	120.592	23.084	11	3.3
2010	4	25	21	50	48.2	120.55	23.066	19	3.1
2010	5	2	18	0	13.5	120.541	22.96	18	4.6
2010	5	11	23	18	31.1	120.676	22.83	19	3.3
2010	5	23	10	20	40.6	120.67	22.826	21	4.3
2010	5	25	4	1	33.3	120.677	22.945	19	3.7
2010	5	29	4	57	40.1	120.599	22.87	18	3.1
2010	6	6	15	29	9.4	120.474	23.18	15	3.9
2010	6	9	19	23	43.2	120.639	22.899	17	3.2
2010	6	16	6	23	46	120.634	22.91	17	4.2
2010	6	22	4	8	54	120.758	23.118	13	3.2

frequency domain, as well as quantity in the time domain at each measuring point of IMFs, can be understood. Here, GPS data at the NS and EW components are both filtered by the frequency band of 5.787×10^{-7} – 7.716×10^{-8} Hz (i.e. 20–150 days in period; for more detail please see Appendix and Chen et al., 2011). Filtered data at the NS component are relative to those of the EW component to yield time-series GPS-azimuths.

4. Analytical results and interpretation

To detect the moving direction of residual displacements, an average is computed from differences of GPS-azimuths orientations between every two stations within a spatially moving region of 80×80 km². Note that the moving window should cover at least 7 GPS stations that can be used to mitigate the influence raised by local tectonic structure in the relative complex Taiwan (Yu et al., 1997; Bos et al., 2003). The GPS index is further determined by an inverse value of the average to yield a proportional relationship with aligned orientations of residual displacements. For example, disordered orientations of GPS-azimuths are caused by either no obvious stress disturbance due to the removal of long-term plate movements from the GPS data, or the approaching to threshold of fault rupture (Chen et al., 2011). In such case, the deduced average would approach 90° and the GPS index is about 0.011 (=1/90°). When earthquake-related stress disturbance accumulates on strata and results in surface displacements toward a similar direction, aligned orientations of

GPS-azimuths will decrease the difference. Thus, the difference-average and the GPS index would yield opposite values, i.e., become small and large, respectively.

Fig. 2 shows time-shifting and spatial-shifting maps of the GPS index from 20 days before to 29 days after the Jiashian earthquake. No significant stress disturbance can be observed from these GPS index maps 11 days before the Jiashian earthquake because of the general low values in GPS index maps (i.e. ~ 0.011 ; the pink color in Fig. 2), except for a small region (23.75°N, 120.5°E). This observation infers that the influence from other small earthquakes prior to the Jiashian event is minimal. It is noted that yellow areas (the average is about 60°; the GPS index is about 0.017) gradually covered southern Taiwan (22.5°N, 120.7°E) 8 days before the Jiashian earthquake. Appearance of yellow areas in this stage suggests that stress in relation to the Jiashian earthquake could gradually disturb on the crust and trigger subsurface movements toward NE direction during 8–1 days before the earthquake. The GPS index remained at the low stage (~ 0.011) regardless intense movements observed nearby the epicenter of the Jiashian earthquake. Generally, pink areas with the GPS index ~ 0.011 were extended from the epicenter toward the NE direction (i.e. from 24.2°N, 120.3°E to 23.0°N, 120.7°E) during 7–3 days before the earthquake. This feature suggests that subsurface displacements toward the NE direction seemed to be impeded near the epicenter of the Jiashian earthquake during this stage. Then, it is found that stress persistently pushed on strata regardless the impeded region and

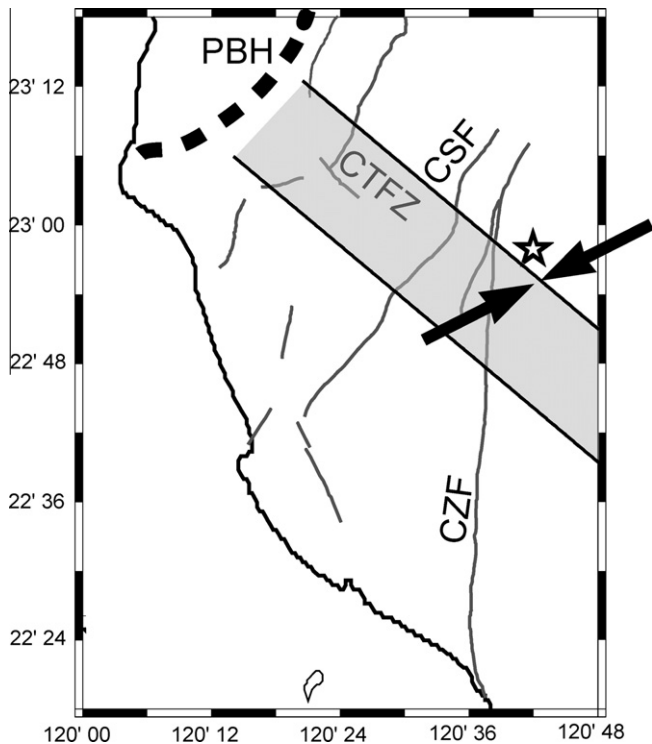


Fig. 3. The schematic diagram of the seismogenic process related to the Jiashian earthquake. The star shows the location of the Jiashian mainshock. The gray lines represent the locations of the main faults in the research area. CSF: the Chishan fault. CZF: the Chaozhou fault. PBH: Peikang basement high. The grey belt is represented as the Chishan Transfer Fault Zone (CTFZ).

consequently exceeded the threshold of a blind fault to trigger the Jiashian earthquake. Note that the epicenter was exactly located at the SE margin (i.e. face) of the impeded region.

In the period of 3–9 days after the earthquake, no significant phenomena of aligned GPS-azimuths can be observed in most areas of Taiwan, except a rectangle region with GPS index about 0.017 existed on the northern side from the epicenter. Note that the NW–SE trend of the rectangle area was consistent with the strike of the blind fault and in an agreement with aftershocks' distribution. The high GPS index ~ 0.017 changed through time. During 10–16 days after the mainshock, the high GPS index ~ 0.017 were extended again and orientations of subsurface displacement moved toward the opposite direction (i.e. the SW direction) before the earthquake. Over the next ten days (i.e. 10–20 days) after the earthquake, areas with significant surface displacements (i.e. the GPS index ~ 0.017) are distributed at the eastern sides of the epicenter along with insignificant surface displacements (i.e. the GPS index ~ 0.011) located at the western side formed as a NW–SE trend. Finally, when detectable stress disturbance associated with the Jiashian earthquake were mitigated over time, the low GPS index (~ 0.011) was well covered all over Taiwan and suggests a relative calm stage with no significant stress disturbance.

5. Discussion and conclusions

Co-seismic displacements along ruptured faults that were excited by earthquakes with small magnitude and/or deep focal depth are normally considered small and are difficult to be detected by using GPS. On the other hand, area of stress accumulation, which triggers fault rupture and earthquakes, has not been

fully comprehended in a seismogenic process. Since GPS-azimuth evolution retrieved from filtered surface displacements is not associated with co-seismic signals, we have an opportunity to examine relationships between changes of the GPS index and parameters of the focal mechanism in the case of the Jiashian earthquake. The aligned orientations of GPS-azimuths observed in most areas in Taiwan was about 70° (i.e. NNE) before the earthquake that has an agreement with the most compressive axis (243°) retrieved from the focal mechanism of the Jiashian earthquake. In contrast, an inverse direction (i.e. SSW) derived from aligned GPS-azimuth appeared 10 days after the earthquake. These aligned directions are orthogonal to the strike of the fault that agrees with common cognition of stress changes associated with thrust earthquakes (Wen et al., 2012; Chan and Wu, 2012; Lee et al., in press). Furthermore, the inverse change of the aligned GPS-azimuth before and after the earthquake is consistent to the seismic rebound theory (Reid, 1910), and as demonstrated in the previous study (Chen et al., 2011). Thus, GPS-azimuth evolution shown in this study is highly related with the focal mechanism retrieved from the Jiashian earthquake with a focal depth of 22 km. Chen et al. (2011) also reported that an agreement between GPS-azimuth evolution and fault parameters can be observed from the M7 earthquake (21.67°N , 120.56°E , on December 26, 2006) about 200 km away. These results suggest that area under stress change, which triggers fault rupture, should be much larger than the rupture zone to fault slip during an earthquake. GPS-azimuth evolution would thus be very useful to evaluate the potential area under earthquake-related stress change during a seismogenic process.

On the other hand, as seismic activity reflects subsurface changes of stress disturbance; the location of aftershocks should be highly related to distribution of GPS index values because the GPS maps can reflect an accurate picture beneath the Earth's surface. Here, we sketched aftershocks of the Jiashian earthquake over the time-shifting GPS index maps to examine their relationships (Fig. 2). It is clear that these aftershocks were aligned along either the strike of fault and/or the southern boundary of the rectangle area during the first ten days after the Jiashian earthquake. Lacombe et al. (2001) purposed that a seismic zone would lead to the NW–SE compression forming the left-lateral rupture behavior (i.e. the Chishan Transfer Fault Zone (CTFZ), see Fig. 3, grey belt) in southern Taiwan (also see Rau and Wu, 1995; Bos et al., 2003; Wen et al., 2012). Residual surface displacements aligned as a NNE–SSW trend 7–1 days before and after the Jiashian earthquake (Fig. 2) imply the existence of the WNW–ESE blind fault that also agrees with the same rupture behavior within CTFZ. This suggests that orientations of GPS-azimuths can generate an accurate picture beneath the surface once the effects of short-term noise, long-term plate movements as well as semi-annual and annual variations can be removed.

In conclusion, filtered surface displacements do reflect nature of stress changes (retrieved from the survey of most thrust faults in Taiwan) even if it is resulted from a blind thrust fault. Average difference values computed from orientations of GPS-azimuths are a good indicator to understand subsurface stress changes. The spatial-shifting GPS index maps show that stress disturbance near the epicenter was impeded a few days before the Jiashian earthquake. Meanwhile, time-shifting maps constructed by the GPS index are very helpful to understand activity of distinct tectonic structures in the vicinity of the epicenter after the earthquake. These results not only provide more detailed information of surface deformation in this specific event, but also can compare well with data retrieved from other earthquakes to clarify discrepancy either in seismogenic processes or post-seismic stress changes.

Acknowledgements

The authors would like to thank the Central Weather Bureau of Taiwan for the whole dataset used in the analyses of this study and the National Science Council of the Republic of China for financially supporting this research under Contract Nos. NSC 100-2116-M-001-027-MY3 and NSC 100-2116-M-001-005.

Appendix A

Fig. A1. shows intrinsic mode functions (IMFs) decomposed from the surface displacement data at the NS component of the HUAL station. To understand characteristics of each IMF, we compute the median instantaneous frequency (Table A1) from entire

points of IMF. IMFs initially decomposed from data are generally in high frequency and noisy mode, such as IMF_{1-5} , which have similar median instantaneous frequencies, are determined to be the noise. Thus, the high bound of the filter band is given by 5.787×10^{-7} Hz (i.e. 20 days in period). To avoid the influence from the semi-annual and annual variations as well as long-term plate movements, the low bound of the filter band is determined as 7.716×10^{-8} Hz (IMF_{12-13} , i.e. 150 days in period). We extract the filtered data from the GPS at NS and EW components in every station using the determined frequency band (i.e. IMF_{6-11}). Meanwhile, filtered data at the EW components are relative to them at the NS components to yield the GPS-azimuth (i.e. horizontal azimuth). Orientations of the deduced GPS-azimuth are further employed in studying distribution of stress changes during the Jiashian earthquake.

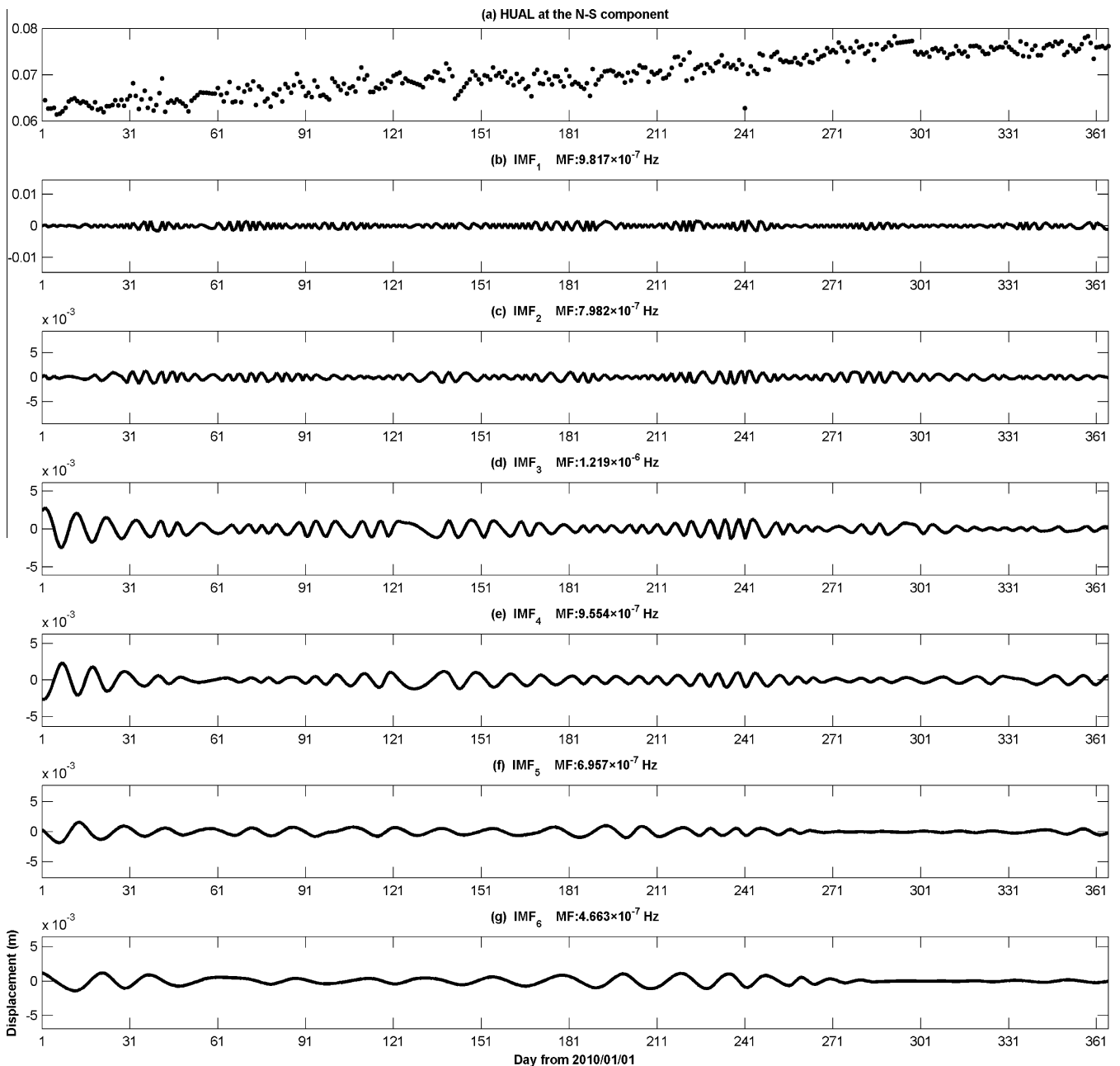


Fig. A1. Thirteen IMFs and the residual derived by HHT from decomposition of the North–South component of GPS position of the HUAL station. MF denotes the median instantaneous frequency of each IMF.

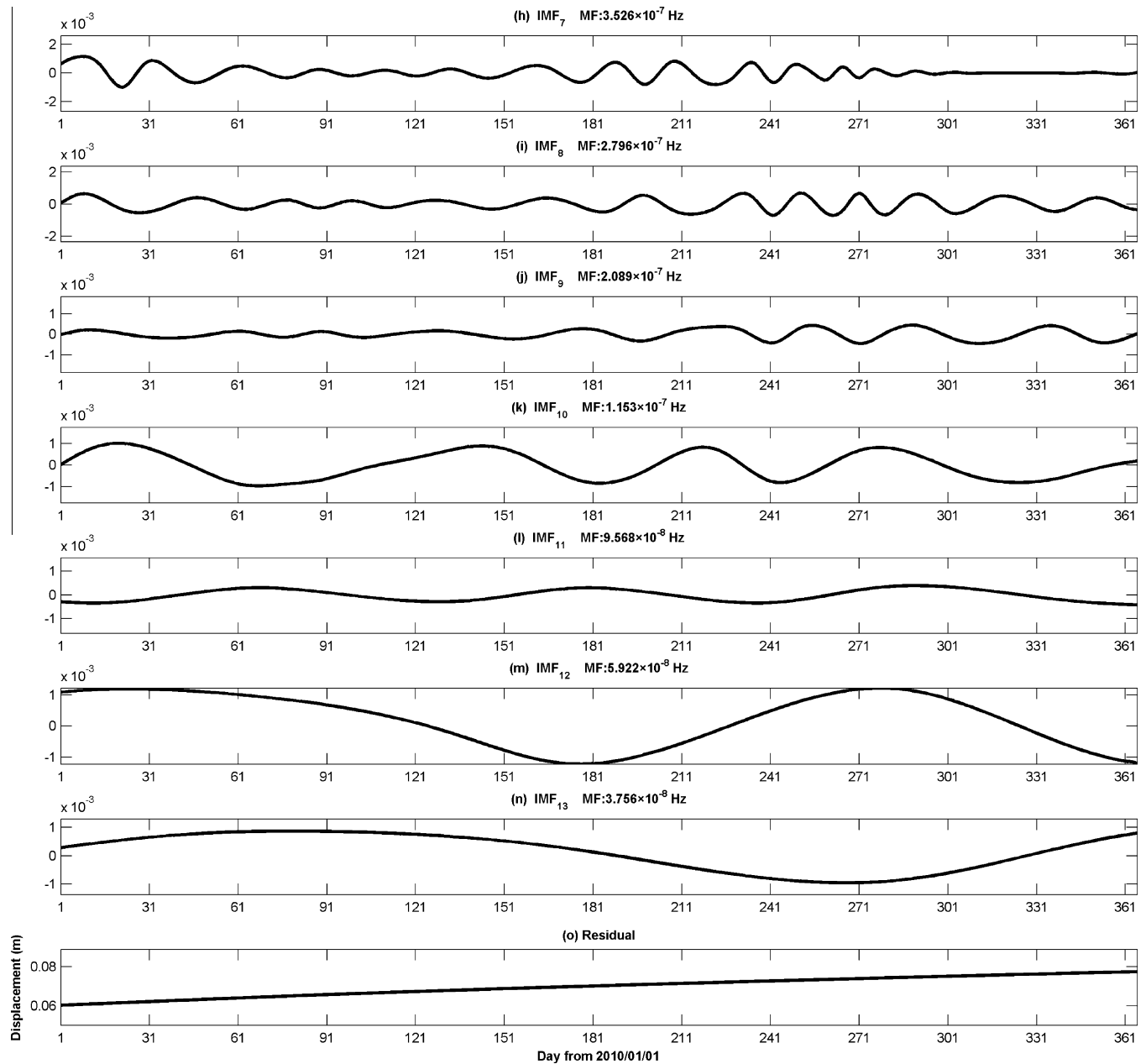


Fig. A1. (continued)

Table A1
Median frequency and period for 13 IMFs in Fig. A1.

IMFs	Median frequency (Hz)	Median period (days)
1	9.817×10^{-7}	11.79
2	7.982×10^{-7}	14.50
3	1.219×10^{-6}	9.49
4	9.554×10^{-7}	12.11
5	6.956×10^{-7}	16.64
6	4.663×10^{-7}	24.82
7	3.526×10^{-7}	32.82
8	2.796×10^{-7}	41.39
9	2.089×10^{-7}	55.41
10	1.153×10^{-7}	100.35
11	9.568×10^{-8}	120.97
12	5.922×10^{-8}	195.44
13	3.756×10^{-8}	308.18

References

- Barbot, S., Fialko, Y., 2010. A unified continuum representation of post-seismic relaxation mechanisms: semi-analytic models of afterslip, poroelastic rebound and viscoelastic flow: semi-analytic models of postseismic transient. *Geophys. J. Int.* 182, 1124–1140.
- Barbot, S., Hamiel, Y., Fialko, Y., 2008. Space geodetic investigation of the coseismic and postseismic deformation due to the 2003 M_w 7.2 Altai earthquake: implications for the local lithospheric rheology. *J. Geophys. Res.* 113, B03403.
- Blewitt, G., Lavallee, D., 2002. Effect of annual signals on geodetic velocity. *J. Geophys. Res.* 107(B7). doi: 10.1029/2001JB000570.
- Bos, A.G., Spakman, W., Nyst, M.C.J., 2003. Surface deformation and tectonic setting of Taiwan inferred from a GPS velocity field. *J. Geophys. Res.* 108(B10), 2458. doi: 10.1029/2002JB002336.
- Bracewell, R.N., 2000. *The Fourier Transform and Its Applications*, third ed. McGraw-Hill, Boston, Mass, pp. 624.
- Chan, C.H., Wu, Y.M., 2012. A seismicity burst following the 2010 $M_6.4$ Jiashian earthquake – implications for short-term seismic hazards in southern Taiwan. *J. Asian Earth Sci.* 59, 231–239. <http://dx.doi.org/10.1016/j.jseaes.2012.08.01>.
- Chen, C.H., Yeh, T.K., Liu, J.Y., Wang, C.H., Wen, S., Yen, H.Y., Chang, S.H., 2011. Surface deformation and seismic rebound: implications and applications. *Surv. Geophys.* 32, 291–313. <http://dx.doi.org/10.1007/s10712-011-9117-3>.

- Ching, K.E., Johnson, K.M., Rau, R.J., Chuang, R.Y., Kuo, L.C., Leu, P.L., 2011. Inferred fault geometry and slip distribution of the 2010 Jiashian, Taiwan, earthquake is consistent with a 312 thick-skinned deformation model. *Earth Planet. Sci. Lett.* 301, 78–86. <http://dx.doi.org/10.1016/j.epsl.2010.10.021>.
- Dach, R., Hugentobler, U., Fridez, P., Meindl, M., 2007. Bernese GPS Software Version 5.0. Astronomical Institute, University of Bern, Bern, Switzerland, pp. 612.
- Daubechies, I., 1990. The wavelet transform time-frequency localization and signal analysis. *IEEE Trans. Inform. Theory* 36, 961–1004.
- Gahalaut, V.K., Nagarajan, B., Catherine, J.K., Skumar, S., 2006. Constraints on 2004 Sumatra Andaman earthquake rupture from GPS measurements in Andaman-Nicobar Islands. *Earth Planet. Sci. Lett.* 242, 365–374.
- Geirsson, H., Árnadóttir, T., Völksen, C., Jiang, W., Sturkell, E., Villemin, T., Einarsson, P., Sigmundsson, F., Stefánsson, R., 2006. Current plate movements across the Mid-Atlantic Ridge determined from 5 years of continuous GPS measurements in Iceland. *J. Geophys. Res.* 111, B09407. <http://dx.doi.org/10.1029/2005JB003717>.
- Ho, C.S., 1988. An introduction to the geology of Taiwan, second ed. Central Geological Survey, The Ministry of Economic Affairs, Taipei, pp. 192.
- Huang, N.E., Wu, Z., 2008. A review on Hilbert–Huang transform: method and its applications to geophysical studies. *Rev. Geophys.* 46, RG2006. <http://dx.doi.org/10.1029/2007RG000228>.
- Huang, N.E., Shen, Z., Long, S.R., Wu, M.C., Shih, H.H., Zheng, Q., Yen, N.-C., Tung, C.C., Liu, H.H., 1998. The empirical mode decomposition and the Hilbert spectrum for nonlinear and non-stationary time series analysis. *Proc. Royal Soc. Lond., Series A: Math., Phys. Eng. Sci.* 454, 903–995.
- Huang, N.E., Shen, Z., Long, S.R., Shen, S.S.P., Hsu, N.H., Xiong, D., Qu, W., Gloersen, P., 2003. On the establishment of a confidence limit for the empirical mode decomposition and Hilbert spectral analysis. *Proc. Royal Soc. Lond., Series A: Math. Phys. Eng. Sci.* 459, 2317–2345.
- Lacombe, O., Mouthereau, F., Angelier, J., Deffontaines, B., 2001. Structural, geodetic and seismological evidence for tectonic escape in SW Taiwan. *Tectonophysics* 333, 323–345.
- Lee, S.-J., Mozziconacci, L., Liang, W.-T., Hsu, Y.-J., Huang, W.-G., Huang, B.-S., In press. Source complexity of the 4 March 2010 Jiashian, Taiwan, Earthquake determined by joint inversion of teleseismic and near field data. *J. Asian Earth Sci.* <http://dx.doi.org/10.1016/j.jseae.2012.11.018>.
- McClusky, S., Reilinger, R., Mahmoud, S., Ben Sari D., Tealeb, A., 2003. GPS constraints on Africa (Nubia) and Arabia plate motions. *Geophys. J. Int.* 155, 126–138. doi: 10.1046/j.1365-246X.2003.02023.x.
- Peltzer, G., Rosen, P., Rogez, F., Hudnut, K., 1998. Poroelastic rebound along the Landers 1992 earthquake surface rupture. *J. Geophys. Res.* 103 (B12), 30131–30145. <http://dx.doi.org/10.1029/98JB02302>.
- Prawirodirdjo, L., Bock, Y., 2004. Instantaneous global plate motion model from 12 years of continuous GPS observations. *J. Geophys. Res.* 109, B08405. <http://dx.doi.org/10.1029/2003JB002944>.
- Rau, R.-J., Wu, F.T., 1995. Tomographic imaging of lithospheric structures under Taiwan. *Earth Planet. Sci. Lett.* 133, 517–532.
- Ray, J., Altamimi, Z., Collilieux, X., Van Dam, T., 2008. Anomalous harmonics in the spectra of GPS position estimates. *GPS Solutions* 12, 55–64.
- Reid, H.F., 1910. The mechanics of the earthquake. In: *The California Earthquake of April 18, 1906, Report of the State Earthquake Investigation Commission, Vol. 2*, Carnegie Institution, Washington, DC, pp. 1–192.
- Reilinger, R.E., McClusky, S.C., Oral, M.B., King, R.W., Toksoz, M.N., Barka, A.A., Kinik, I., Lenk, O., Sanli, I., 1997. Global positioning system measurements of present-day crustal movements in the Arabia–Africa–Eurasia plate collision zone. *J. Geophys. Res.* 102 (B5), 9983–9999. <http://dx.doi.org/10.1029/96JB03736>.
- Saastamoinen, J., 1973. Contributions to the theory of atmospheric refraction. *Bull. Géodésique* 107, 13–34.
- Van Dam, T., Wahr, J., Milly, P.C.D., Shmakin, A.B., Blewitt, G., Lavalée, D., Larson, K.M., 2001. Crustal displacements due to continental water loading. *Geophys. Res. Lett.* 28, 651–654.
- Wang, K., 2007. Elastic and viscoelastic models of crustal deformation in subduction earthquake cycles. In: Dixon, T.H., Moore, J.C. (Eds.), *The Seismogenic Zone of Subduction Thrust Faults, MARGINS Theoretical and Experimental Earth Science Series*. Columbia University press, New York, USA, pp. 545–575.
- Wang, C.S., Liou, Y.A., Yeh, T.K., 2008. Impact of surface meteorological measurements on GPS height determination. *Geophys. Res. Lett.* 35, L23809. <http://dx.doi.org/10.1029/2008GL035929>.
- Wen, S., Hsu, H.J., Chang, W.Y., Chen, C.H., 2012. A study of the seismogenic process beneath the south-western foothills in Taiwan in relation with the 2010 Jiashian earthquake. *Tectonophysics*. <http://dx.doi.org/10.1016/j.tecto.2012.06.029>.
- Wernicke, B., Davis, J.L., Bennett, R.A., Normandeau, J.E., Friedrich, A.M., 2004. Tectonic implications of a dense continuous GPS velocity field at Yucca Mountain, Nevada. *J. Geophys. Res.* 109, B12404. <http://dx.doi.org/10.1029/2003JB002832>.
- Yeh, T.K., Hwang, C., Xu, G., 2008. GPS height and gravity variations due to ocean tidal loading around Taiwan. *Surv. Geophys.* 29, 37–50.
- Yeh, T.K., Hwang, C., Xu, C., Wang, C.S., Lee, C.C., 2009. Determination of global positioning system (GPS) receiver clock errors: impact on positioning accuracy. *Meas. Sci. Technol.* 20, 075105. <http://dx.doi.org/10.1088/0957-0233/20/7/075105>.
- Yu, S.B., Chen, H.Y., Kuo, L.C., 1997. Velocity field of GPS stations in the Taiwan area. *Tectonophysics* 274, 41–59.
- Yu, S.B., Kuo, L.C., Hsu, Y.J., Su, H.H., Liu, C.C., Hou, C.S., Lee, J.F., Lai, T.C., Liu, C.C., Liu, C.L., Tseng, T.F., Tsai, C.S., Shin, T.C., 2001. Preseismic deformation and coseismic displacements associated with the 1999 Chi–Chi, Taiwan earthquake. *Bull. Seismol. Soc. Am.* 91, 995–1012.